Holocene variability of East Asian summer monsoon as viewed from the speleothem $\delta^{18}O$ records in central China

Yanjun Cai[1,2,3], Xing Cheng[1,4], Le Ma[1], Ruixue Mao[1], Sebastian F.M. Breitenbach[5], Haiwei Zhang[2], Gang Xue[1,4], Hai Cheng[2,6], R. Lawrence Edwards[6], Zhisheng An[1,3]

1. State Key Laboratory of Loess and Quaternary Geology, Institute of Earth Environment, Chinese Academy of Science, Xi'an 710061, China
2. Institute of Global Environmental Change, Xi'an Jiaotong University, Xi'an 710049, China
3. Open Studio for OCCEC, Qingdao National Laboratory for Marine Science and Technology, Qingdao, China
4. University of Chinese Academy of Sciences, Beijing 100049, China
5. Department of Geography and Environmental Sciences, Northumbria University, NE1 8ST, United Kingdom
6. Department of Earth Sciences, University of Minnesota, Minneapolis, Minnesota 55455, USA

Corresponding Author: Yanjun Cai, yanjun_cai@xjtu.edu.cn

Abstract

Monsoon precipitation in East China shows distinct spatial distribution and its variability is closely linked with the changes of the East Asian summer monsoon (EASM). Located in the transition zone between the southern subtropical humid climate and the northern warm temperate semi-humid climate, central China is a core region for recognizing and understanding the spatio-temporal variability of the EASM. Using U-series dating and stable isotope analysis on five stalagmites (MG-1, MG-2, MG-7, MG-40 and MG-64) from Magou Cave, Henan Province, Central China, we construct a high-resolution and precisely dated composite stalagmite $\delta^{18}O$ time series covering most of the Holocene. This composite record reveals variations in precipitation $\delta^{18}O$ between 11.7 and 1.1 ka BP with average resolution of ~4 years. The Magou composite record demonstrates that EASM intensity dominates long-term changes in precipitation $\delta^{18}O$, which generally follows the northern hemisphere summer insolation (NHSI) trend. Both, Ensemble Empirical Mode Decomposition (EEMD) and wavelet filtering analyses real that the amplitudes of long-term (100-500 and 500-3000 years) components were slightly reduced between 8.5 and 4.9 ka BP, implying a weakened influence of climatic forcings on centennial and even millennial timescales during this warm period. Variance on 1-30-year timescales is relatively low and ascribed to sampling resolution. Fourteen weak EASM intervals, including the 8.2 ka event, were identified within the period corresponding broadly with the Holocene Megathermal. Since no cold excursions other than the 8.2 ka event are found in the Greenland ice core records, we tentatively propose that oscillations in tropical sea surface temperature (SST) likely play an important role in steering other weak monsoon events. Aligning the Magou composite record and other moisture records with archaeological records from the study region, it seems that climate

change influenced both the spatial distribution and agricultural practices of ancient cultures. However, overall moderate climatic changes in this region, most likely characterized by shifts between subtropical humid climate and warm temperate semi-humid climate, supported a generally consecutive development of ancient cultures without major hiatuses.

Keywords: Stalagmite, Central China, Stable Isotopes, East Asian Summer Monsoon, Variability, Holocene

1. Introduction

Increasing attention has been paid to the Holocene, the most recent geological chronozone, owing to close links of past climatic and environmental changes with the development of human civilizations, and the resemblance of the middle Holocene to future global climate conditions. In East Asia, numerous archives, including loess, lakes, peats, stalagmites, and sand-dune deposits have been used to study the history and variability of Holocene climate and environmental changes (An et al., 2000, 2012; Dykoski et al., 2005; Hong et al., 2003; Hu et al., 2008; Li et al., 2007; Wang et al., 2005; Xiao et al., 2004; Yang et al., 2019). Holocene temperature reconstructions from East Asia show generally consistent changes, i.e., relatively high temperatures during the early and middle Holocene, with the period of 8.5-3.3 ka called the Holocene Megathermal, and a subsequent gradual decrease throughout the late Holocene (Fang et al., 2011; Ge et al., 2007; Shi et al., 1992;), although some studies suggest a persistent temperature increase from the early to the late Holocene (Hou et al., 2019; Liu et al., 2014a;). However, precipitation (or effective precipitation) reconstructions show significant spatial variability. For example, already in 2000, An et al. (2000) proposed an asynchronous Holocene Optimum Period from north to south China, largely defined by the peak of effective precipitation. Subsequently, Ran and Feng (2013) proposed a gradual, lagged, increase of precipitation from south to north in eastern China. These studies largely focused on the characteristics of long-term changes throughout the Holocene, while few studies discussed climate events on centennial to decadal scales.

Detailed analysis of modern meteorological observations shows significant regional differences in monsoon precipitation across eastern China (Ding, 2009). The region is

characterized by a dipole mode, with southern flood and northern drought and *vice versa* at decadal timescales. An additional sandwich pattern of arid central conditions, bracketed by wetter conditions to the north and south, and *vice versa*, also likely recurred over the instrumental observed period. An important question then is whether such spatial pattern existed in the past, and at what time scales and how they are manifested in geological records? The lack of well-dated high-resolution records complicates the study of centennial- to decadal-scale climate dynamics and hinders the understanding of spatial variation of monsoon precipitation and limits assessing future climatic and environmental changes at these timescales.

The climate change has substantial impacts on the development of ancient cultures (deMenocal, 2001, and references therein; Weiss, et al., 1993). Beyond all doubt, the rise and fall of Neolithic cultures in China were closely linked with Holocene climate change. Notably, the documented cultural remains reveal a continuum of cultural periods prior to historical dynasties during the Holocene (from ~10.5 ka to ~3.5 ka) in the central plains of China, without significant hiatuses between different cultural periods (Li et al., 2013; Li et al., 2015a; Wang, 2014), a scenario quite different from that in northern China (Li et al., 2007; Yang et al., 2015). Why are the cultural remains so widely distributed in this central region and why are there no distinct cultural shifts/hiatuses? Clarifying the relationship between the continued activity of early civilizations and climate change might help adaptation and mitigation efforts to ease societal vulnerability against climatic changes. A deeper understanding of these climate-societal interrelationships requires a network of proximal well-dated records of climatic and environmental dynamics from high-fidelity sites in the central plains of China.

To help fill this gap, we present a precisely dated and highly resolved (temporal resolution of 3-10 years) stalagmite isotope records from Magou Cave, Henan Province, central China (figure 1). We reconstruct the Holocene history of the EASM, characterize the climate instability during the Holocene Megathermal and investigate possible physical mechanisms behind the climatic changes in the study region. Finally, we examine possible links between civilization succession and climate change.

2. Cave site and local climate

Magou Cave (113°23’E, 34°19’N, 422 m above sea level) is located 50 km southwest of Zhengzhou City, Henan Province, China (figure 1). The cave formed in the Ordovician limestone of the Ju-Ci-Shan Group. It was a closed cave without natural entrance before it has been exposed and destroyed during quarrying activities in 2010. The annual mean temperature is about 14.4℃, and the annual precipitation varies between 421.3 and 1121.4 mm, with a mean of 721.2 mm from 1953-2010, as observed at the nearest Xuchang meteorological station (113°52’E, 34°2’N, 47 km southeast of the Cave site, http://www.geodata.cn). Precipitation falls mainly during the summer monsoon season, with about 62% of the annual budget delivered between June and September.

Straddling the boundary between the subtropical humid zone and the warm temperate semi-humid zone in China, the EASM dictates the local climate and environment. In summer, southerly winds from the low latitudes prevail and provide important monsoonal precipitation; in winter, northerly winter monsoon winds bring cold, dry

air from mid- to high-latitudes regions (figure 1), defining a cold and relatively dry winter climate regime. With these alternations of the summer and winter monsoons, a distinctly warm-humid summer and cold-dry winter seasonality governs this region (Cwa climate according to the Koeppen-Geiger classification, Peel et al. 2007).

The special geographical location of the cave leads to the heightened climate sensitivity of this area, and the Central plain is the core region of agricultural production and of great significance to China's food security (The Editorial Committee of China Agricultural Statistical Yearbook, 2017). Regional climate change has a significant impact on agricultural production (Wang et al., 2007). Therefore, the study of climate dynamics in this region is of great significance not only for understanding the spatial variability of Holocene climate across Eastern China, but also for projecting and coping with future climate change.

3. Stalagmites and methods

Five stalagmites, MG-1, MG-2, MG-7, MG-40 and MG-64 have been retrieved from Magou Cave and are for this study. After halving these stalagmites (figure 2 shows the polished sections of the five stalagmites), about 50-60 mg powder subsamples were drilled along the growth axis of each stalagmite and prepared for ^{230}Th-^{234}U-^{238}U dating. The chemical separating procedure for uranium and thorium is similar to that described in Edwards et al. (1987), and the details on instrumental measuring protocols can be found in Cheng et al. (2013). A $^{230}Th/^{232}Th$ atomic ratio of $4.4\pm2.2\times10^{-6}$ was used to correct for initial ^{230}Th. The measured data, the decay constants and the calculated ages are listed in supplementary Table 1.

The micro-milling approach was used to extract sub-samples at different sampling resolution. For stalagmite MG-1, the sampling intervals are 50 μm between 0 and 3.6 mm, 100 μm for the interval 3.6-7.6 mm, and 150 μm between 7.6 and 225.15 mm; for stalagmite MG-2, the sampling intervals are 100 μm in the portion of 0-15 mm and 200 μm between 15 and 139.6 mm. In stalagmites MG-40, MG-7 and MG-64 the sampling intervals are 50 μm, 100 μm and 100 μm, respectively. A total of 3846 oxygen and carbon stable isotope analyses were performed using an IsoPrime 100 mass spectrometer equipped with a Multi-Prep Device at the Institute of Earth Environment of the Chinese Academy of Sciences. All oxygen and carbon isotope results are reported in delta (δ) notation. The standard results show that the precision of $\delta^{18}O$ and $\delta^{13}C$ analyses are better than 0.15‰ and 0.12 ‰ (2σ), respectively.

The stable isotope data and most dates from stalagmites MG-1 and MG-40 have been reported in an earlier study (Mao et al. 2016). Here we report two additional dates from the base of MG-40, and five more dates from stalagmite MG-1 which improved their chronologies significantly.

4. Results

4.1 The U/Th chronology

In total, sixty-six ^{230}Th dates were attained from the five stalagmites, with 23 dates from MG-1, 11 dates from MG-2, 13 dates from MG-7, 8 dates from MG-40 and 11 dates from stalagmite MG-64. Given the high density of dates and relatively small dating errors (most errors are <1%) and with most dates in stratigraphic order (figure 3), we use linear interpolation to establish depth-age chronologies for each stalagmite. We also use the COPRA routine (Breitenbach et al., 2012) to test the reliability of the

linear chronology and find negligible differences between both approaches (figure 3). The modeled chronologies indicate that MG-1 spans the time period from 4.88-10.36 ka, MG-2 from 5.84-7.77 ka, MG-40 from 6.91-11.48 ka and MG-64 from 1.11-5.43 ka. The ^{230}Th dates obtained from stalagmite MG-7 show three growth periods, i.e., from ~78.70 to 77.39 ka, 11.80 to 10.13 ka, and between ~8.20 and 7.74 ka. In this study, we focus only on the Holocene section (11.80 to 10.13 ka) to attain the highest resolved isotope profiles. The growth intervals of these stalagmites overlap for different time windows (figure 3a).

The calculated growth rates of these stalagmites vary from 1.2 μm/year to 500 μm/year, with mean growth rates of 41.1 μm/year, 72.3 μm/year, 18.9 μm/year, 5.2 μm/year and 19.0 μm/year for stalagmites MG-1, MG-2, MG-7, MG-40 and MG-64, respectively. The large variability observed in mean growth rates suggests that the growth-controlling mechanisms (e.g. water pathway through the epikarst, drip rate, degree of supersaturation of the dripwater, CO_2 degassing) differed for these stalagmites. As shown in figure 3b, higher growth rates largely occurred during the mid-Holocene (~8.0 - 4.8 ka BP), implying optimum conditions for speleothem calcite deposition existed at the time.

4.2 The $\delta^{18}O$ and $\delta^{13}C$ records

Using the aforementioned micro-milling intervals, we achieved a mean temporal resolution of 3.5 years, 2.5 years, 5.3 years, 9.2 years and 5.3 years for stalagmites MG-1, MG-2, MG-7, MG-40 and MG-64, respectively, as calculated from their chronologies. As shown in figure 4a, $\delta^{18}O$ varied from -7.8‰ to -12.8‰ in all stalagmites. Generally, $\delta^{18}O$ decreased abruptly after 11.7 ka BP, and then gradually, until 9.2 ka BP, without a clear long-term trend between 9.2 and 5.0 ka BP. Between

5.0 and 3.3 ka BP the $\delta^{18}O$ record consistently trended towards higher values. After 3.3 ka BP, the $\delta^{18}O$ values first decreased and then followed an increasing trend. Superimposed on this long-term trend are prominent large-amplitude decadal-scale oscillations. We build a composite $\delta^{18}O$ record (MG-composite, figure 5) by combining the best dated and highest resolved sections of the individual $\delta^{18}O$ time series of the five stalagmites of the overlapping periods. This composite $\delta^{18}O$ record covers most of the Holocene, i.e., from 11.80 to 1.11 ka, with an average temporal resolution of ~4 years.

The $\delta^{13}C$ records range from -7.0‰ to -11.5‰ and their variability largely follows that of $\delta^{18}O$, showing first a decreasing trend, then a stabilization during the mid-Holocene, and finally increased and more variable values during the late Holocene (figure 4b). The $\delta^{13}C$ values of stalagmite MG-40 are systematically ~1.0-1.2‰ heavier compared to those of stalagmites MG-1 and MG-7 during the overlap period ~8.0 to ~11.5 ka BP, implying that the factors that influence the $\delta^{13}C$ signal differ among the stalagmites.

5. Discussion

5.1 Testing for isotope equilibrium deposition

Given that the cave had no direct connection with the surface, both ventilation and potential for evaporation in the cave were minimal, providing an exceptionally stable microclimatic environment for the deposition of speleothem calcite under (near-)isotope-equilibrium conditions. Within the quoted chronological confidence limits, and considering the differences in temporal resolution, all $\delta^{18}O$ time series show remarkable similarities during the overlapping interval between 11.7 and 5 ka

BP (figure 4a). The new time series also share similarities with a composite Holocene $\delta^{18}O$ record from Laomudong/Dongshiya Caves (figure 5a, Zhang et al., 2018), both situated ~180 km southwest of Magou Cave, and a Holocene $\delta^{18}O$ record from Jiuxian Cave, located ~400 km west of Magou Cave (figure 5b, Cai et al., 2010). The replication of all the $\delta^{18}O$ records suggests that these stalagmites were very likely deposited under (near-)isotopic equilibrium conditions and influenced by similar environmental processes (Dorale and Liu, 2009; Wang et al., 2001).

Our four stalagmites also show consistent variations in the $\delta^{13}C$ profiles in the overlapping period (figure 4b), which supports the replication test discussed above, although the $\delta^{13}C$ values of stalagmite MG-40 are systematically about 1.0-1.2 ‰ higher relative to those in stalagmites MG-1 and MG-7 over the interval prior ~8.1 ka BP. This offset might result from differences in the proportion of seepage versus fracture flow feeding the stalagmites. Higher $\delta^{13}C$ values in sample MG-40 might indicate a larger influence of prior calcite precipitation in the epikarst in a faster-emptying fracture-flow setting.

The different lines of evidence outlined above suggest that the samples from Magou Cave were deposited with minimal kinetic influence and that their stable isotope records primarily reflect regional scale climatic variability.

5.2 The interpretation of speleothem calcite $\delta^{18}O$

Stalagmite $\delta^{18}O$ is jointly controlled by $\delta^{18}O$ of dripwater (which reflects the sum of all factors that control the water from its source to the stalagmite), and the temperature inside the cave, provided that the stalagmite was formed under

(near-)isotopic equilibrium conditions (Hendy, 1971). Regarding the speleothem $\delta^{18}O$ changes found in our stalagmites it is clear that temperature alone is insufficient to explain the observed ca. five per mil amplitude. Experimental studies and theoretical calculations (Coplen, 2007; Kim and O'Neil, 1997; O'Neil et al., 1969,) showed that the temperature-dependent oxygen isotope fractionation between calcite and water is about -0.23‰/°C. For northern China a lowering in annual mean temperature of about 2-3°C has been estimated from the warmest Holocene thermal maximum to the coldest period of the Little Ice Age (Wang et al., 2001b). Thus, temperature changes would explain at most ~0.7‰ of the observed $\delta^{18}O$ change in our records. Using the cave-specific empirical water–calcite oxygen isotope fractionation relationship of -0.177‰/°C of Tremaine et al. (2011) would reduce the explained change in speleothem $\delta^{18}O$ further to only ~0.5‰. Thus, the observed changes in the Holocene $\delta^{18}O$ time series from Magou Cave are mainly governed by the $\delta^{18}O$ signal of the dripwater, i.e., by the history of the supplied moisture and related variations in the amount-weighted $\delta^{18}O$ of meteoric precipitation above the cave.

It is worth to noting that we cannot strictly exclude any temperature effect on the variation of speleothem calcite $\delta^{18}O$ because the variation of precipitation $\delta^{18}O$ might be slightly altered by the temperature-dependent fractionation between dripwater and speleothem calcite. Also, the Holocene temperature conundrum (Liu et al., 2014a), i.e., the inconsistency between reconstructed cooling and inferred warming forced by GHGs and ice sheet, limits our ability to constrain the temperature contribution to variations in speleothem calcite $\delta^{18}O$. We argue that changes in precipitation $\delta^{18}O$ outweighed potential temperature effects, due to the small temperature-dependent fractionation and low overall Holocene temperature changes (~2-3°C in

reconstructions, Wang et al., 2001, and ~1.5-2℃ in model simulations, Liu et al., 2014a).

In monsoonal East Asia, multiple factors have been shown to affect the $\delta^{18}O$ of dripwater (i.e. amount-weighted $\delta^{18}O$ of precipitation, changes in summer : winter precipitation ratio (Wang et al., 2001), rainout between tropical oceanic sources and the cave sites (Yuan et al., 2004), changes in the fraction of summer monsoon rainfall with low $\delta^{18}O$ signal of the annual total (Cheng et al., 2009), and moisture source changes (Cai et al., 2001, 2015; Tan, 2014)). The $\delta^{18}O$ signal in precipitation in the EASM region reflects changes in the $\delta^{18}O$ of atmospheric vapor in the upstream source regions over the Indian ocean (Baker et al. 2015; Liu et al., 2014b; Maher, 2008). Cai et al. (2017) further demonstrated that upstream convection, rather than moisture source change, causes interannual variation in ASM precipitation $\delta^{18}O$ values, corroborating the importance of the rainout effect on the isotopic composition of precipitation. It should be noted that the mentioned rainout effect does not mean that monsoonal precipitation $\delta^{18}O$ is negatively correlated with local rainfall amount at all sites (i.e. the "amount effect", Dansgaard 1964), but rather Rayleigh fractionation along the moisture transport pathway(s). Taken together, the rainout history of moisture transported to the cave is essential for the interpretation of speleothem calcite $\delta^{18}O$. Lower $\delta^{18}O$ values generally indicate more distal moisture source(s) in tandem with enhanced *en route* rainout linked to a stronger summer monsoon and vice versa. Here, we largely follow the explanation by Cheng et al. (2016) and use the terms 'strong monsoon' and 'weak monsoon' to refer to low and high speleothem $\delta^{18}O$ values, respectively. We are cognizant of the argument that changes in circulation and moisture sources (Cai et al., 2010, 2015; Hoffmann and

Heimann, 1997), and changes in recycling may contribute significantly to precipitation $\delta^{18}O$ in our study region. We will discuss their influences in detail later.

5.3 Variability of speleothem $\delta^{18}O$ on different timescales

The MG-composite $\delta^{18}O$ profile spans the time period from 11.7 to 1.1 ka BP and displays distinct variability on different timescales. At the beginning of the reconstruction at ~11.7 ka BP, $\delta^{18}O$ values are relatively heavy (~-8.2 ‰). A shift toward more depleted values occurred between 11.7 and ~11.5 ka BP, largely corresponding with the end of the Younger Dryas event (Brauer et al., 2008). Following this decrease, the $\delta^{18}O$ time series decreased gradually to -10.5 ‰, along with large amplitude oscillations until ~9.25 ka BP. Thereafter, $\delta^{18}O$ fluctuated around a mean value of -10.5 ‰ (stdev ±0.42, 1 σ) till ~5.0 ka BP, with a negligible long-term trend of +0.03 ‰/1000 a. From ~5.0 ka BP to ~3.6 ka BP, the $\delta^{18}O$ record quickly increased to ca. -9.8 ‰, with superimposed decadal to multi-decadal large amplitude oscillations. Between ~3.4 ka BP and 2.7 ka BP, $\delta^{18}O$ values increased ca. 1.2 ‰ to the highest observed values of the entire time series, and then decreased again until ca. 2.2 ka BP. After 2 ka BP and to the end of the record the $\delta^{18}O$ values increased about 1 ‰.

To separate the modes of variability in the MG composite $\delta^{18}O$ time series we applied Ensemble Empirical Mode Decomposition (EEMD) analysis method (Wu and Huang, 2009). Using this method, we obtain a total of 13 intrinsic functions (IFs, figure 6b-h). The combined IFs 13-10 explain 20.3% of the variance and hint at variations of the $\delta^{18}O$ reconstruction on sub-orbital timescales (figure 6b). IFs 9-8 (~26.1% of the variance) show variability on timescales from sub-millennial to millennial years (figure 6c). The combined IFs 7-6 (~22.7% of the total variance) display MG $\delta^{18}O$

variation at centennial timescales (figure 6d). IFs 5-4 vary on multi-decadal timescales (figure 6f) and explain ~19.5% of the variance of the record. Finally, IFs 3-1 show the decadal and shorter oscillations during periods with high growth rate (figure 6h); these IFs include also some noise and must be treated with care.

We used a wavelet filter approach to further inspect the output of the EEMD analysis. As shown in figure 6, the residual component, the 3000-500 year, 500-100 year, and 100-30 year band-pass outputs are highly correlated with the combined IFs 13-10, IFs 9-8, IFs 7-6, and IFs 5-4, with correlation coefficients of 0.96, 0.83, 0.90 and 0.92 (all p values< 0.01) respectively, confirming that the combined intrinsic functions reflect the variability of the MG composite $\delta^{18}O$ record on different timescales. Additionally, the 1-30 years band-pass output is similar to the combined functions of IFs 1-3, showing high-frequency oscillations of the MG-composite $\delta^{18}O$ record.

Comparison of the different IF variance with each other suggests comparable variability of the precipitation $\delta^{18}O$ (under the assumption that speleothem $\delta^{18}O$ mainly reflects precipitation $\delta^{18}O$), on different timescales. Although IFs 1-3 could explain ~11.4% of the record's variance, there is no discernible or distinct variation during periods of low growth rate, highlighting the importance of record resolution on the identification of sub-decadal variability. However, the IF 1-3 record reveals some periods that reach annual to multi-annual resolution, even if age uncertainties hinder us from discussing their variability in detail. The combined IFs 6-7 and IFs 8-9 (i.e., variations on 100-500- and 500-3000-years timescales) show slightly lower amplitudes between ~8.5 and 4.9 ka BP, a period broadly aligned with the Holocene Megathermal (Shi et al., 1992; Wang et al., 2001b). The EEMD analyses of the

published $\delta^{18}O$ records from nearby caves, i.e. LM/DSY and Jiuxian caves, show the similar patterns in general (supplementary figure 1&2). This feature demonstrates relatively stable climatic conditions at centennial to millennial timescales during this warm time interval.

It is worth noting that higher $\delta^{18}O$ values centered at 1.4, 3.2, 4.3, 6.1, 8.1, 9.9, and 10.7 ka BP, indicative of weakened summer monsoon, align with the observed 500-3000 years variability. These events agree with weak EASM events identified across East Asia (Donges et al. 2015; Hong et al., 2003; Wang et al., 2005;), confirming suggested links to dynamics in the North Atlantic (Bond et al., 2001, figure 6c). The variability in the 100-500 years band (IFs 6-7, figure 6d) might be linked to shifts in the mean position of the ITCZ in response to lower solar activity, but further work is required to understand the underlying forcing (Gray et al. 2010 and references therein). Meanwhile, the combined IFs 4-5 functions, comparable with the 30-100 years band-pass output, do not show such long-term pattern. Instead these IFs highlight similar amplitude changes throughout the entire record, indicating continued multi-decadal variability of the precipitation-driven $\delta^{18}O$ record. Exceptions with lower amplitude are observed in periods with reduced deposition rates: ~11.7-10.7 ka BP, ~10.1-8.6 ka BP, and ~2.8-1.1 ka BP. We tentatively propose that there are no significant changes in the multi-decadal variability of the precipitation $\delta^{18}O$ signal, implying relatively stable variability of Asian summer monsoon at multi-decadal timescales which may be largely forced by the interaction of internal factors of climate systems. While the IF results indicate continuous *relative* variability at these timescales, high-resolution records with extreme age control are needed to test this proposition.

5.4 Spatial variability of Holocene speleothem $\delta^{18}O$ across East Asian monsoon regions

The spatial feature of Holocene climate change in China, in particular, the Holocene Optimum, has been first explored by An et al. (2000), subsequently by Ran and Feng (2013), and recently by Zhou et al. (2016). However, no satisfactory mechanism has been identified to interpret the observed phenomena in a holistic way.

Various Holocene speleothem $\delta^{18}O$ records have been reported from south to north China over the last 20 years (Cai et al., 2001; Hu et al., 2008; Wang et al., 2005; Yang et al., 2019, reference therein; Zhang et al., 2018). These records are essential to understand the spatial variability of Holocene environmental conditions across East Asia. Recently, Yang et al. (2019) have tried to combine all Chinese Holocene speleothem $\delta^{18}O$ records into a single synthetic composite record, as well as to compare synthetic records for southern and northern China. They find that all the Holocene speleothem records share a common long-term trend, confirming the dominant control of NHSI on EASM dynamics. However, significant disparity still exists between southern and northern China. As shown in Fig. 4 in Yang et al. (2019), the composite speleothem $\delta^{18}O$ record from northern China (Fig. 4e) started to increase much later (ca. 5.3 ka BP) than the composite record from southern China (Fig. 4d) (it should be pointed out that the original figure in Yang et al. (2019) mixed up the composite records of northern and southern China, personally confirmed with Dr. YANG Xunlin, the corresponding author). Comparing the Holocene speleothem $\delta^{18}O$ record from Jiuxian Cave, central China, with other cave records from southern China, Cai et al. (2010) found that the increasing trend in $\delta^{18}O$ over the Holocene

commenced earlier in the southern monsoonal region, and later at higher latitudes. Here, we compare the speleothem $\delta^{18}O$ records from three sites in central China, i.e. Magou Cave, Dongshiya/Laomu caves, and Jiuxian Cave (figure 5). Within quoted errors and considering the differences in resolution, these three records replicate their millennial-scale to centennial variability. All three records indicate that speleothem $\delta^{18}O$ was relatively lower during the early and middle Holocene (from ~9.0 to 5.0 ka BP) and without a long-term trend, and only after ~5.0 ka BP speleothem $\delta^{18}O$ started to increase, further corroborating the pattern proposed by Cai et al. (2010).

Why then do speleothem $\delta^{18}O$ records suggest an extended 'Holocene Moisture Optimum' in northern China? We hypothesize that this can be explained by changes in precipitation $\delta^{18}O$, which largely reflects the fraction of water vapor rained out between tropical sources and the cave. The difference of the $\delta^{18}O$ in precipitation between two sites from south to north can reflect the rainout between these two sites (Hu et al., 2008), supposing there were no significant changes in moisture sources or kinetic effects. Thus, the delayed increase of speleothem $\delta^{18}O$ in northern China suggests that during the late mid-Holocene an increased fraction of water vapor rained out between the southern (Heshang Cave) and central China sites (Magou Cave) (supplementary figure 3). Some researchers argued that the increase of speleothem $\delta^{18}O$ reflects a decreasing contribution of moisture from the Indian Ocean, or that rainout upstream of the Indian monsoon region was reduced (Maher, 2008). This is not at odds with our interpretation of increased precipitation in northern China during the mid-Holocene, because we are concerned only about the precipitation $\delta^{18}O$ difference between (southern) upstream sites and Magou Cave. Taking all these lines of evidence together, and consistent with reconstructions based on other archives

from central and northern China (Chen et al., 2015; Xiao et al., 2004; Wei et al., 2020), it is likely that precipitation was higher from 8.5 ka BP to 5.3 ka BP, which could be regarded as the Holocene Moisture Optimum in central China, and diminished in the second half of the Holocene.

It is worth noting that two factors substantially influence the precipitation estimate. One is the amount of moisture transported, because the precipitation amount is the function of both available moisture and the fraction of water vapor that is rained out. Another factor is the contribution of recycled water, because if sufficient recycled water is available, the $\delta^{18}O$ signal of the water vapor *en route* might remain the same (Rozanski et al., 1993). An increased contribution of recycled water would lead to underestimation of precipitation amount. Increased temperature would lead to increased atmospheric specific humidity and also increase evapotranspiration. It is likely that from the early to mid-Holocene moisture transport and recycling were increased, and that the precipitation $\delta^{18}O$ difference between sites alone may underestimate the amount of precipitation during the middle Holocene. How and to what degree these two factors affect the estimate of precipitation amount during the Holocene warrants further study, including sophisticated model simulations. We recognize that changes in moisture source might also affect the precipitation amount estimate on a single trajectory. However, we refrain from further discussion, because we qualitatively estimate the precipitation amount on a generally consistent trajectory using the precipitation $\delta^{18}O$ difference between the upstream and cave sites across a larger region. The likelihood of a changed moisture source seems relatively small compared to other factors.

5.5 Variation of precipitation $\delta^{18}O$ during the Holocene Megathermal and its implications

During the Holocene, a period warmer than present, namely the Holocene Megathermal (Fairbridge, 2009), has been identified around the northern Hemisphere, albeit of variable timing and different amplitudes of temperature in different regions (Johnsen et al., 2001; Kaufman et al., 2004; Shi et al., 1992; Wang, 2011). In China, Shi et al. (1992) suggested that the Holocene Megathermal occurred between 8.5 and 3.0 ka BP, and the temperature increase may have been as high as 3℃ in northern China and only 1℃ in southern China. It has also been suggested that this warm period was not consistently warm and stable, but rather variable (Fang et al., 2011; Ge et al., 2007; Peng et al., 2005; Wang et al., 2001b). Some discrepancies are apparent, probably due to the different spatial domains and chronological control (He et al., 2004).

Here we investigate the variability of speleothem $\delta^{18}O$ during this Holocene warm period in more detail. Between 8.5 and 4.9 ka BP the $\delta^{18}O$ record from stalagmite MG-1 shows a very weak and hardly discernable long-term trend (figure 7), similar to the components identified with the EEMD and wavelet filtering analysis (IFs $_{10+11+12+12+13}$ and residual in figure 6), indicating stable long-term climatic conditions in central China. However, large-amplitude (1.0-1.5 per mil) high-frequency (intra-decadal to multi-decadal) oscillations characterize this period. With the 15-year weighted-average time series of the MG-1 $\delta^{18}O$ record, fourteen weak monsoon intervals (namely WMI 1 to WMI1 4) are identified with trough values exceeding 1.5 standard deviations of the mean of this interval (similar to the 8.2 event) (figure 7c).

The ages of the mid-points of these events are 8.29 ka BP, 8.12 ka BP, 7.71 ka BP, 7.67 ka BP, 7.35 ka BP, 7.08 ka BP, 6.57 ka BP, 6.25 ka BP, 6.08 ka BP, 6.00 ka BP, 5.79 ka BP, 5.50 ka BP, 5.35 ka BP, 5.18 ka BP. Within quoted dating uncertainty, these events could align with the events identified from the $\delta^{18}O$ record from Dongge Cave (figure 7b), and comparable fluctuations could be found in the $\delta^{18}O$ record from Heshang Cave (figure 7a), although the amplitudes of these events are varied in different records. The durations of these events varied from ~20 to ~70 years. The weak monsoon interval 2, centered at 8.12 ka BP, lasted ca. 50 years, and is most likely related to the 8.2 ka event (Cheng et al., 2009b; Liu et al., 2013). This WMI 2 shows a double-plunging structure if take the small trough at ~8.20 ka BP into consideration. The 8.2 ka BP event is the most prominent Holocene excursion observed in the Greenland ice cores (Alley et al., 1997). Its manifestation in Asian monsoon precipitation $\delta^{18}O$ has been suggested to be brought about via a cold and extended Siberian High, resulting in a southward shift of the mean position of the ITCZ (Cheng et al., 2009b; Liu et al., 2013; Wang et al. 2004; Wang et al., 2005).

However, the amplitude of the 8.2 ka BP WMI 2 is the same or even smaller than other weak monsoon intervals identified during the Holocene Megathermal, suggesting that the variability of precipitation $\delta^{18}O$ in central China is affected by other processes as well. A 200 year long, seasonally-resolved speleothem $\delta^{18}O$ record from Dongshiya Cave (Zhao et al., 2018), suggests that, on annual to decadal timescales, speleothem $\delta^{18}O$ (and by inference precipitation $\delta^{18}O$) in central China is related to the West Pacific Subtropical High (WPSH, Zhao et al., 2018), i.e., high $\delta^{18}O$ values indicate a westward extension of the WPSH, and vice versa. If this relation was still valid during the Holocene Megathermal, the identified WMIs may

be associated with substantial variations of the WPSH. Changes in the WPSH have been linked to the SST in the tropical Indian Ocean and West Pacific (Sun and Ying, 1999; Wang et al., 2000; Wu et al., 2010; Xie et al., 2009). Others suggested that changes in the WPSH might result via feedback processes from the EASM domain (Hoskins, 1996; Liu et al., 2001). Recently, Fan et al. (2018) reported a high-resolution SST time series from west Pacific warm pool. It indicates that there were substantial variations of SST on centennial timescale (figure 7d), hinting the potential linkage between the WMIs and temperature change in West Pacific, although we cannot line up these oscillations in SST with WMIs in our record one by one due to lower resolution and relatively larger age uncertainties of SST record. Considering that both, tropical SST and the EASM system play an important role in WPSH dynamics, and that no significant excursions (except the 8.2 ka event) associated with the WMIs are found in the northern high latitudes, we tentatively propose that these WMI could be associated with surface temperature changes in the tropical Indian Ocean and West Pacific, and that considerable SST changes occurred on centennial timescale during the Holocene Megathermal.

5.6 Variation of speleothem calcite $\delta^{13}C$ and its climate significance

The $\delta^{13}C$ is a valuable proxy reflecting local environmental changes (Fohlmeister et al., 2020; Lechleitner et al., 2017). Multiple factors (either individually or in combination) may contribute to the speleothem $\delta^{13}C$ signal, including the isotopic composition of soil CO_2, which reflects the vegetation activity and composition (i.e., C_3 vs C_4), the biomass, and microbial activity in the soil, dissolution of carbonate rock (open system vs. closed system), and prior carbonate precipitate (PCP) in the epikarst and/or the cave environment (Genty et al., 2006; Fohlmeister et al., 2020; Lechleitner et al., 2017; McDermott, 2004; Ridley et al., 2015). As shown in figure 4, the long-

term $\delta^{13}C$ variations generally share similarities with $\delta^{18}O$, indicating both $\delta^{13}C$ and $\delta^{18}O$ were affected by common forcings on different timescales, most likely reflecting changes in local effective rainfall associated with the summer monsoon intensity. Lower $\delta^{13}C$ values indicate intensified effective EASM rainfall and enhanced soil CO_2 production and reduced PCP in the epikarst above the cave, whereas higher values result from reduced microbial activity in the soil, and enhanced PCP under drier conditions. While vegetation and soil dynamics likely play a role for the multi-centennial to millennial scale trend in $\delta^{13}C$, the higher-frequency changes are probably more directly related to PCP changes. The $\delta^{13}C$ profile also features centennial-multi-decadal scale environmental changes that mirror those observed in the $\delta^{18}O$ time series. This fact corroborates the notion that local moisture changes are directly related to regional EASM dynamics (Liu et al., 2014b). There are also several periods (e.g. 10.8-11.4 ka BP and 3.6-4.2 ka BP) showing anti-phase variation or disparities in the $\delta^{13}C$ and $\delta^{18}O$ records. It's likely caused by the closed system dissolution (Genty et al., 2001) resulted from the increased precipitation. However, these inferences are only tentative and independent evidence (e.g. PCP-sensitive trace element ratios) is required to verify this interpretation.

5.7 Potential impact of climate change on cultural development in central China

The relationship between climate and the fate of ancient cultures has long been the research focus in academia. By aligning records of climate change and archeological observations, many researches have linked the hiatus or 'collapse' of ancient cultures to large and persistent climatic and environmental changes (Carolin et al. 2019; Chen et al., 2005; Cullen et al. 2000; deMenocal, 2001; Haug et al., 2003; Hodell et al., 1995; Kennett et al., 2012; Sinha et al., 2019; Weiss et al., 1993; Yang et al., 2015; Zhang et al., 2008).

Located in the Central Plain with favorable climate and environment, Henan Province is rich in Neolithic archaeological sites. Different to other regions in China, the Neolithic cultures in this region (figure 8a) are consecutively developed without cultural dislocation (Li et al., 2015a). However, these cultures still experienced significant changes. While during the Lijiagou period only few Neolithic archeological sites have been recorded in Henan Province, the number of sites increased slightly during the Peiligang period, and subsequently significantly during both the Yangshao and Longshan periods, while their number decreased strongly during the Erlitou period (Li et al., 2013). Spatially, archaeological sites are concentrated along the middle and lower reaches of rivers in western and central Henan during the Peiligang and Erlitou periods, while during the Yangshao and Longshan periods sites were dispersed more widely from the hilly to the lower plains. The changes in the number of sites and their spatial distribution suggest that climatic changes could have been an important factor influencing cultural development in Henan province. Intensified EASM and increased precipitation, as indicated by our stable isotope records (both $\delta^{18}O$ and $\delta^{13}C$), the growth frequency of the stalagmites from Longfeng Cave (Wei et al., 2020) and the reconstructed precipitation using the pollen records extracted from lake sediments (Chen et al., 2015, figure 8), and higher temperatures during the early Holocene (10.5-7 ka BP, not shown here, Wang et al., 2001) likely provided favorable environmental conditions for the development of the Lijiagou to Peiligang cultures and supported the prosperous development of the Yangshao and Longshan cultures. Reduced precipitation, possible in tandem with lower temperatures, might have hastened the decline of the Erlitou culture, as

indicated by the reduced number of sites and distribution patterns in Henan Province (Li et al., 2013).

Furthermore, changes in planted crop species and pollen assemblages suggest climate change may have affected Neolithic cultural development in Henan Province. Plant remains from Baligang site, Dengzhou in Henan Province, indicate that during the Peiligang culture period the population cultivated rice and gathered fruits (Deng and Gao, 2012). Subsistence strategies then changed to adopt a mixture of rice, foxtail millet and common millet during the Yangshao and Longshan cultures with variable proportions of these three crops, i.e., relatively increased millets during the early Yangshao and late Longshan periods (Deng and Gao, 2012; Fu et al., 2010;). At the same time, millets (adapted to drier climate compared to rice) are widely grown at the northern sites. An increased proportion of millets likely suggests drier conditions during the early Yangshao and the late Longshan periods, consistent with the inference of precipitation changes from our stable isotope records and other proxy records (figure 8), although we cannot exclude the potential influence of interplay between northern foxtail millet-based cultures (i.e., Yangshao and Longshan) and southern rice-growing cultures (i.e., Jujialing and Shijiahe) (Li et al., 2015b).

Taken together, it is most likely that the relatively moderate climatic shifts in Henan Province, i.e., changes from subtropical humid to warm temperate semi-humid climate, generally allowed consecutive development of ancient cultures in the Central Plain, but modulated the livelihood and adaptation measures of these cultures.

6. Conclusions

As the transition zone between the subtropical humid and the warm temperate semi-humid climates, and today dominated by the summer monsoon, the central plain of China is a core area of modern agricultural production, as well as ancient civilization. At the same time, this region is sensitive to climate change. Based on the high-precision U-series-based chronologies from five stalagmites we developed highly resolved stable isotope time series covering the period from ~11.7 to 1.1 ka BP with an average resolution of ~4 years.

The new composite record reveals changes in precipitation $\delta^{18}O$ and demonstrates that summer monsoon intensity dominated the long-term dynamics of precipitation $\delta^{18}O$, which followed NHSI. EEMD and wavelet analysis show comparable variance of precipitation $\delta^{18}O$ on different timescales. Variance on timescales of 1-30 years is relatively low, reflecting the influence of the record's temporal resolution on these timescales. The reduced amplitudes of the 100-500 years and 500-3000 years components imply muted climate variability between 8.5-4.9 ka BP. Fourteen weak monsoon intervals were identified in this period, which largely corresponds to the Holocene Megathermal. Some of the identified weak monsoon intervals reveal positive $\delta^{18}O$ excursions larger than that associated with the 8.2 ka event. In the absence of cold excursions, as inferred for the 8.2 ka event, these EASM oscillations are tentatively linked to changes in tropical SST.

Aligning this record with archaeological observations, it seems likely that climatic changes influenced the development of ancient cultures. However, the moderate

622 regional climatic change during the discussed part of the Holocene allowed
623 continuous development of ancient cultures in Henan Province, central China.
624

625 Acknowledgements

626 We thank two anonymous reviewers for their thoughtful suggestions. This work was
627 supported by the National Key Research and Development Program of China
628 (2017YFA0603401), the Strategic Priority Research Program of Chinese Academy of
629 Sciences (Grant No. XDB 40010200) and National Natural Science Foundation of
630 China grants (41888101), and the Young Talent Support Plan of Xi'an Jiaotong
631 University.

References

Alley, R.B., Mayewski, P.A., Sowers, T., Stuiver, M., Taylor, K.C., Clark, P.U., 1997. Holocene climatic instability: Aprominent, widespread event 8200 yr ago. Geology 25(6), 483-486.

An, Z., Porter, S.C., Kutzbach, J.E., Wu, X., Wang, S., Liu, X., Li, X., Zhou W., 2000. Asynchronous Holocene optimum of the East Asian monsoon. Quaternary Science Reviews 19, 743-762.

An, Z., Colman, S.M., Zhou, W., Li, X., Brown, E.T., Jull, A.J.T., Cai, Y., Huang, Y., Lu, X., Chang, H., Song, Y., Sun, Y., Xu, H., Liu, W., Jin, Z., Liu, X., Cheng, P., Liu, Y., Ai, L., Li, X., Liu, X., Yan, L., Shi, Z., Wang, X., Wu, F., Qiang, X., Dong, J., Lu, F., Xu, X., 2012. Interplay between the Westerlies and Asian monsoon recorded in Lake Qinghai sediments since 32 ka. Scientific Reports 2,619

Bond, G., Kromer, B., Beer, J., Muscheler, R., Evans, M.N., Showers, W., Hoffmann, S., Lotti-Bond, R., Hajdas, I., Bonani, G., 2001. Persistent Solar Influence on North Atlantic Climate During the Holocene. Science 294, 2130-2136.

Breitenbach, S.F.M., Rehfeld, K., Goswami, B., Baldini, J.U.L., 2012. Constructing proxy records from age models (COPRA). Climate of the Past 8, 1765e1779.

Cai, Y., Zhang, M., Peng, Z., Lin, Y., An, Z., Zhang, Z., Cao, Y., 2001. The $\delta^{18}O$ variation of a stalagmite from Qixing Cave, Guizhou Province and indicated climate change during the Holocene. Chinese Science Bulletin 46(22), 1904-1908.

Cai, Y., Tan, L., Cheng, H., An, Z., Edwards, R.L., Kelly, M.J., Kong, X., Wang, X., 2010. The variation of summer monsoon precipitation in central China since the last deglaciation. Earth and Planetary Science Letters 291, 21-31.

Cai, Y., Fung, I.Y., Edwards, R.L., An, Z., Cheng, H., Lee, J.-E., Tan, L., Shen, C.-C., Wang, X., Day, J.A., 2015. Variability of stalagmite-inferred Indian monsoon precipitation over the past 252,000 y. Proceedings of the National Academy of Sciences 112, 2954-2959.

Cai, Z., Tian, L., Bowen, G.J., 2017. ENSO variability reflected in precipitation oxygen isotopes across the Asian Summer Monsoon region. Earth and Planetary Science Letters 475, 25-33.

Carolin, S.A., Walker, R.T., Day, C.C., Ersek, V., Sloan, R.A., Dee, M.W., Talebian, M., Henderson, G.M., 2019. Precise timing of abrupt increase in dust activity in the Middle East coincident with 4.2 ka social change. Proceedings of the National Academy of Sciences 116, 67-72.

Chen, F., Xu, Q., Chen, J., Birks, H.J.B., Liu, J., Zhang, S., Jin, L., An, C., Telford, R.J., Cao, X., Wang, Z., Zahng, X., Selvaraj, K., Lü, H., Li, Y., Zheng, Z., Wang, H., Zhou, A., Dong, G., Zhang, J., Huang, X., Bloemendal, J., Rao, Z., 2015. East Asian summer monsoon precipitation variability since the last deglaciation. Scientific Reports http://dx.doi.org/10.1038/srep11186.

Chen, Z., Wang, Z., Schneiderman, J., Taol, J., Cail, Y., 2005. Holocene climate fluctuations in the Yangtze delta of eastern China and the Neolithic response. The Holocene 15, 915-924.

Cheng, H., Edwards, R.L., Broecker, W.S., Denton, G.H., Kong, X., Wang, Y., Zhang, R., Wang, X., 2009a. Ice Age Terminations. Science 326, 248-252.

Cheng, H., Fleitmann, D., Edwards, R.L., Wang, X., Cruz, F.W., Auler, A.S., Mangini, A., Wang, Y., Kong, X., Burns, S.J., Matter, A., 2009b. Timing and

678 structure of the 8.2 kyr B.P. event inferred from $\delta^{18}O$ records of stalagmites from
679 China, Oman, and Brazil. Geology 37, 1007-1010.

680 Cheng, H., Lawrence Edwards, R., Shen, C.-C., Polyak, V.J., Asmerom, Y.,
681 Woodhead, J., Hellstrom, J., Wang, Y., Kong, X., Spötl, C., Wang, X., Calvin
682 Alexander Jr, E., 2013. Improvements in ^{230}Th dating, ^{230}Th and ^{234}U half-life values,
683 and U–Th isotopic measurements by multi-collector inductively coupled plasma mass
684 spectrometry. Earth and Planetary Science Letters 371–372, 82-91.

685 Cheng, H., Edwards, R.L., Sinha, A., Spötl, C., Yi, L., Chen, S., Kelly, M., Kathayat,
686 G., Wang, X., Li, X., 2016. The Asian monsoon over the past 640,000 years and ice
687 age terminations. Nature 534, 640-646.

688 Coplen T., 2007. Calibration of the calcite–water oxygen-isotope geothermometer at
689 Devils Hole, Nevada, a natural laboratory. Geochimica et Cosmochimica Acta 71,
690 3948–3957.

691 Cullen, H.M., deMenocal, P.B., Hemming, S., Hemming, G., Brown, F.H.,
692 Guilderson, T., Sirocko, F., 2000. Climate change and the collapse of the Akkadian
693 empire: Evidence from the deep sea. Geology 28, 379-382.

694 Deevey, E.S., and Flint, R.F., 1957. Postglacial Hypsithermal interval. Science, 125,
695 182–185.

696 deMenocal, P.B., 2001. Cultural Responses to Climate Change During the Late
697 Holocene. Science 292, 667-673.

698 Den, Z.H. and Gao, Y., 2012, The analysis of archaeobotanical remains from
699 Baligang site, Dengzhou, Henan Province. Cultural Relics in Southern China, 1:162-
700 169. In Chinese with English Abstract.

Ding, Y., Sun, Y., Wang, Z., Zhu, Y., Song, Y., 2009. Inter- decadal variation of the summer precipitation in China and its association with decreasing Asian summer monsoon Part II: Possible causes. International Journal of Climatology 29, 1926-1944.

Donges, J.F., Donner, R., Marwan, N., Breitenbach, S.F., Rehfeld, K., Kurths, J., 2015. Non-linear regime shifts in Holocene Asian monsoon variability: potential impacts on cultural change and migratory patterns. Climate of the Past 11, 709-741.

Dorale, J.A., Liu, Z., 2009. Limitations of Hendy test criteria in judging the paleoclimatic suitability of speleothems and the need for replication. Journal of Cave and Karst Studies 71, 73-80.

Dreybrodt, W., 2008. Evolution of the isotopic composition of carbon and oxygen in a calcite precipitating H_2O-CO_2-$CaCO_3$ solution and the related isotopic composition of calcite in stalagmites. Geochimica et Cosmochimica Acta 72, 6198-6198.

Dykoski, C.A., Edwards, R.L., Cheng, H., Yuan, D., Cai, Y., Zhang, M., Lin, Y., Qing, J., An, Z., Revenaugh, J., 2005. A high-resolution, absolute-dated Holocene and deglacial Asian monsoon record from Dongge Cave, China. Earth and Planetary Science Letters 233, 71-86.

Edwards, R.L., Chen, J., Wasserburg, G.J., 1987. ^{238}U-^{234}U-^{230}Th-^{232}Th systematic and the precise measurement of time over the past 500,000 years. Earth and Planetary Science Letters 81, 175-192.

Fairbridge, R.W., 2009. Hypsithermal, in: Gornitz, V. (Ed.), Encyclopedia of Paleoclimatology and Ancient Environments. Springer Netherlands, Dordrecht, pp. 451-452.

Fan, W., Jian, Z., Chu, Z., Dang, H., Wang, Y., Bassinot, F., Han, X., Bian, Y., 2018. Variability of the Indonesian Throughflow in the Makassar Strait over the Last 30 ka. Scientific Reports 8, 5678.

Fang, X., Hou, G., 2011. Synthetically reconstructed Holocene temperature change in China. Scientia Geographica Sinica 31, 385-393. In Chinese with English abstract.

Fohlmeister, J., Riavo G. Voarintsoa, N., Lechleitner, F.A., Boyd, M., Brandtstätter, S., Jacobson, M.J., Oster, J., 2020. Main Controls on the Stable Carbon Isotope Composition of Speleothems, Geochimica et Cosmochimica Acta, doi: https://doi.org/10.1016/j.gca.2020.03.042.

Fu, X., Jin, S., Hu, Y., Ma, Z., Pan, J., Wang, C., Agricultural development and palaeodietary study of Gouwan site, Xichuan, Henan. Chinese Science Bulletin, 2010, 55: 614-620, doi: 10.1007/s11434-009-06215

Ge, Q., Wang, S., Wen, X., Shen, C., Hao, Z., 2007. Temperature and precipitation changes in China during the Holocene. Advances in Atmospheric Sciences 24, 1024-1036.

Genty, D., Blamart, D., Ghaleb, B., Plagnes, V., Causse, C., Bakalowicz, M., Zouari, K., Chkir, N., Hellstrom, J., Wainer, K., Bourges, F., 2006. Timing and dynamics of the last deglaciation from European and North African delta C-13 stalagmite profiles - comparison with Chinese and South Hemisphere stalagmites. Quaternary Science Reviews 25, 2118-2142.

Haug, G.H., Gu¨nther, D., Peterson, L.C., Sigman, D.M., Hughen, K.A., Aeschlimann, B., 2003. Climate and the Collapse of Maya Civilization. Science 299, 1731-1735.

He, Y., Theakstone, W. H., Zhang, Z., Zhang, D., Yao, T., Chen, T., Shen, Y., Pang, H. 2004, Asynchronous Holocene climatic change across China. Quaternary Research, 61, 52–63.

Hendy, C.H., 1971. The isotopic geochemistry of speleothems--I. The calculation of the effects of different modes of formation on the isotopic composition of speleothems and their applicability as palaeoclimatic indicators. Geochimica et Cosmochimica Acta 35, 801-824.

Hodell, D.A., Curtis, J.H., Brenner, M., 1995. Possible role of climate in the collapse of Classic Maya civilization. Nature 375, 391-394.

Hoffmann, G., Werner, M., Heimann, M., 1998. Water isotope module of the ECHAM atmospheric general circulation model: A study on timescales from days to several years. Journal of Geophysical Research, 103 (No. D14): 16871-16896.

Hong, Y., Hong, B., Lin, Q., Zhu, Y., Shibata, Y., Hirota, M., Uchida, M., Leng, X., Jiang, H., Xu, H., 2003. Correlation between Indian Ocean summer monsoon and North Atlantic climate during the Holocene. Earth and Planetary Science Letters 211, 371-380.

Hoskins, B.J., 1996. On the existence and strength of the summer subtropical anticyclones. Bulletin of the American Meteorological Society 77:1287–1292.

Hou, J., Li, C.-G., Lee, S., 2019. The temperature record of the Holocene: progress and controversies. Science Bulletin 64, 565-566.

Hu, C., Henderson, G.M., Huang, J., Xie, S., Sun, Y., Johnson, K.R., 2008. Quantification of Holocene Asian monsoon rainfall from spatially separated cave records. Earth and Planetary Science Letters 266, 221-232.

Johnsen, S., Dahl-Jensen, D., Gundestrup, N., Steffensen, J., Clausen, H., Miller, H., Masson-Delmotte, V., Sveinbjornsdottir, A., White, J., 2001. Oxygen isotope and palaeotemperature records from six Greenland ice-core stations: Camp Century, Dye-3, Grip, GISP2, Renland and Northgrip. Journal of Quaternary Science 16, 299–307.

Kaufman, D.S., Ager, T.A., Anderson, N.J., Anderson, P.M., Andrews, J.T., Bartlein, P.J., Brubaker, L.B., Coats, L.L., Cwynar, L.C., Duvall, M.L., Dyke, A.S., Edwards, M.E., Eisner, W.R., Gajewski, K., Geirsdóttir, A., Hu, F.S., Jennings, A.E., Kaplan, M.R., Kerwin, M.W., Lozhkin, A.V., MacDonald, G.M., Miller, G.H., Mock, C.J., Oswald, W.W., Otto-Bliesner, B.L., Porinchu, D.F., Rühland, K., Smol, J.P., Steig, E.J., Wolfe, B.B., 2004. Holocene thermal maximum in the western Arctic (0–180°W). Quaternary Science Reviews 23, 529-560.

Kennett, D.J., Breitenbach, S.F.M., Aquino, V.V., Asmerom, Y., Awe, J., Baldini, J.U.L., Bartlein, P., Culleton, B.J., Ebert, C., Jazwa, C., Macri, M.J., Marwan, N., Polyak, V., Prufer, K.M., Ridley, H.E., Sodemann, H., Winterhalder, B., Haug, G.H., 2012. Development and Disintegration of Maya Political Systems in Response to Climate Change. Science 338, 788-791.

Kim, S.-T., O'Neil, J.R., 1997. Equilibrium and nonequilibrium oxygen isotope effects in synthetic carbonates. Geochimica et Cosmochimica Acta 61, 3461-3475.

Lechleitner F.A., Breitenbach S.F.M., Cheng H., Plessen B., Rehfeld K., Goswami B., Marwan N., Eroglu D., Adkins J.F., Haug G.H., 2017. Climatic and in-cave influences on $\delta^{18}O$ and $\delta^{13}C$ in a stalagmite from northeastern India through the last deglaciation. Quaternary Research 88, 458-471, doi: 10.1017/qua.2017.72

Li, B., Wen, X., Qiu, S., 2007, Phases of Environmental Evolution Indicated by Primary Chemical Elements and Paleontological Records in the Upper Pleistocene-

Holocene Series for the Salawusu River Valley, China. Acta Geologica Sinica 81(4):555–565

Li, K., Ma, C., Gao, W., Li, S., Li, Z., Pan, Y., 2015a, Progress and trend of Holocene environmental archaeology in Henan Province. Progress in Geography, 34 (7): 883-897, doi: 10.18306/dlkxjz.2015.07.010

Li, X., Shen, H., Tian, J., 2007, The Influences of Environment Evolution on Ancient Culture Development in the Northern Part of China. Journal of Hebei Normal University/Natural Science Edition, 31(5): 680-685. In Chinese with English abstract.

Liu, Y., Henderson, G., Hu, C., Mason, A., Charnley, N., Johnson, K., Xie, S., 2013. Links between the East Asian monsoon and North Atlantic climate during the 8,200 year vent. Nature Geoscience 6, 117-120.

Liu, Y., Wu, G., Liu, H., Liu, P., 2001. Condensation heating of the Asian summer monsoon and the subtropical anticyclone in the Eastern Hemisphere. Climate Dynamics 17(4):327–338

Li, Z., Zhu, C., Wu, G., Zheng, C., Shao, S., Feng, F., Wang, Y., 2013. Spatial and temporal distribution of prehistoric human sites and its driving factors in Henan Province. Acta Geographica Sincia, 68(11): 1527-1537. In Chinese with English Abstract.

Li, Z., Zhu, C., Yuan, S., Xu, J., Wu, G., Wang, H., Guo, Z., 2015b, Geographical distribution, diffusion and subsistence variation of prehistoric cultures in Nanyang Basin, Henan Province. Acta Geographica Sinica, 70(1):143-156. In Chinese with English Abstract.

816 Liu, Z., Zhu, J., Rosenthal, Y., Zhang, X., Otto-Bliesner, B.L., Timmermann, A.,
817 Smith, R.S., Lohmann, G., Zheng, W., Timm, O.E., 2014a. The Holocene temperature
818 conundrum. Proceedings of the National Academy of Sciences 111, E3501-E3505.

819 Liu, Z., Wen, X., Brady, E., Otto-Bliesner, B., Yu, G., Lu, H., Cheng, H., Wang, Y.,
820 Zheng, W., Ding, Y., 2014b. Chinese cave records and the East Asia summer
821 monsoon. Quaternary Science Reviews 83, 115-128.

822 Maher, B.A., 2008. Holocene variability of the East Asian summer monsoon from
823 Chinese cave records: a re-assessment. The Holocene 18, 861-866.

824 Mao, R., Cai, Y., Ma, L., Cheng, X., 2016. Early to mid-Holocene paleoclimatic
825 changes recorded by the stalagmites from the Magou Cave, Henan Province. Journal
826 of Earth Environment, 7(3): 254-268. In Chinese with English abstract.

827 McDermott, F., 2004. Palaeo-climate reconstruction from stable isotope variations in
828 speleothems: a review. Quaternary Science Reviews 23, 901–918.

829 O'Neil, J.R., Clayton, R.N., Mayeda, T.K., 1969. Oxygen isotope fractionation in
830 divalent metal carbonates. The Journal of Chemical Physics 51(12), 5547-5558.

831 Peng, X., Zhong, W., Zhao, Y., Xue, J., 2005. Preliminary research in the Holocene
832 Hypsithermal climate change. Journal of South China Normal University: Natural
833 Science Edition, (2): 52–60.

834 Ran, M., Feng, Z., 2013. Holocene moisture variations across China and driving
835 mechanisms: A synthesis of climatic records. Quaternary International 313, 179-193.

836 Ridley, H.E., Asmerom, Y., Baldini, J.U.L., Breitenbach, S.F.M., Aquino, V.V.,
837 Prufer, K.M., Culleton, B.J., Polyak, V., Lechleitner, F.A., Kennett, D.J., Zhang,
838 M.H., Marwan, N., Macpherson, C.G., Baldini, L.M., Xiao, T.Y., Peterkin, J.L., Awe,

J., Haug, G.H., 2015. Aerosol forcing of the position of the intertropical convergence zone since AD 1550. Nature Geoscience 8, 195-200.

Rozanski, K., Araguas-Araguas, L., Gonfiantini, R., 1993. Isotopic patterns in modern global precipitation. Geophysical Monography 78, 1-36.

Shi, Y., Kong, Z., Wang, S., Tang, L., Wang, F., Yao, T., Zhao, X., Zhang, P., Shi, S., 1992. Basic features of climates and environments during Holocene Megathermal in China. In: Shi, Y.F., Kong, Z.C. (Eds.), The Climates and Environments of Holocene Megathermal in China. China Ocean Press, Beijing, pp. l–18. in Chinese.

Sinha, A., Kathayat, G., Weiss, H., Li, H., Cheng, H., Reuter, J., Schneider, A.W., Berkelhammer, M., Adalı, S.F., Stott, L.D., 2019. Role of climate in the rise and fall of the Neo-Assyrian Empire. Science advances 5, eaax6656.

Sun, S., Ying, M., 1999. Subtropical high anomalies over the western Pacific and its relations to the Asian monsoon and SST anomaly. Advances in Atmospheric Sciences 16, 559-568.

Tan, M., 2014. Circulation effect: response of precipitation $\delta^{18}O$ to the ENSO cycle in monsoon regions of China. Climate Dynamics 42, 1067-1077.

The Editorial Committee of China Agricultural Statistical Yearbook. 2017, China Agriculture Yearbook. China Agriculture Press, Beijing.

Tremaine, D.M., Froelich, P.N., Yang, W., 2011. Speleothem calcite farmed in situ: Modern calibration of $\delta^{18}O$ and $\delta^{13}C$ paleoclimate proxies in a continuously-monitored natural cave system. Geochimica et Cosmochimica Acta 75, 4929-4950.

Wang, B., Wu, R., Fu, X., 2000. Pacific–East Asian teleconnection: how does ENSO affect East Asian climate? Journal of Climate 13, 1517-1536.

862 Wang, J., Zhu, Y., Liu, H., 2007, Main agrometeorological disasters and their impact
863 in recent 28 years in Henan. Meteorological and Environmental Sciences 30, 9-11.

864 Wang, S., Gong, D., Zhu, J., 2001b. Twentieth-century climatic warming in China in
865 the context of the Holocene. The Holocene 11, 313-321.

866 Wang, S., 2011. Holocene Megathermal. Advances in Climate Change Research 7(5):
867 383-384.

868 Wang, X., Auler, A.S., Edwards, R.L., Cheng, H., Cristalli, P.S., Smart, P.L.,
869 Richards, D.A., Shen, C.-C., 2004. Wet periods in northeastern Brazil over the past
870 210 kyr linked to distant climate anomalies. Nature 432, 740-743.

871 Wang, Y., Cheng, H., Edwards, R.L., An, Z., Wu, J., Shen, C.-C., Dorale, J.A., 2001a.
872 A high-resolution absolute-dated late Pleistocene Monsoon record from Hulu cave,
873 China. Science 294, 2345-2348.

874 Wang, Y., Cheng, H., Edwards, R.L., He, Y., Kong, X., An, Z., Wu, J., Kelly, M.J.,
875 Dykoski, C.A., Li, X., 2005. The Holocene Asian Monsoon: Links to Solar Changes
876 and North Atlantic Climate. Science 308, 854-857.

877 Wang Y., 2014. On the research progress of Lijiagou site in Xinmi City and other
878 related problems. Cultural Relics of Central China, (1): 20-24.

879 Wei, Y., Cai, Y., Cheng, X., Xue, G., Lu, Y., Ma, L., Huang, S., He, M., Cheng, H.,
880 Edwards, R.L., 2020. Holocene and deglaciation hydroclimate changes in northern
881 China as inferred from stalagmite growth frequency. Global and Planetary Change
882 195, 103360.

883 Weiss, H., Courty, M.A., Wetterstrom, W., Guichard, F., Senior, L., Meadow, R.,
884 Curnow, A., 1993. The Genesis and Collapse of Third Millennium North
885 Mesopotamian Civilization. Science 261, 995-1004.

Wu, B., Li, T., Zhou, T., 2010, Relative contributions of the Indian ocean and local SST anomalies to the maintenance of the western north Pacific anomalous anticyclone during the El Niño decaying summer. Journal of Climate 23(11):2974–2986

Wu, Z., Huang, N., 2009, Ensemble Empirical Mode Decomposition: A noise-assisted data analysis method. Advances in Data Analysis and Classification 1:1–41.

Xie, S., Hafner, J., Tokinaga, H., Du, Y., Huang, G., Sampe, T., 2009, Indian ocean capacitor effect on Indo-Western Pacific climate during the summer following El Niño. Journal of Climate 22(3):730–747

Xiao, J., Xu, Q., Nakamura, T., Yang, X., Liang, W., Inouchi, Y., 2004. Holocene vegetation variation in the Daihai Lake region of north-central China: a direct indication of the Asian monsoon climatic history. Quaternary Science Reviews 23, 1669-1679.

Yang, X., Scuderi, L.A., Wang, X., Scuderi, L.J., Zhang, D., Li, H., Forman, S., Xu, Q.H., Wang, R., Huang, W., Yang, S., 2015. Groundwater sapping as the cause of irreversible desertification of Hunshandake Sandy Lands, Inner Mongolia, northern China. Proceedings of the National Academy of Sciences 112, 702-706.

Yang, X., Yang, H., Wang, B., Huang, L.-J., Shen, C.-C., Edwards, R.L., Cheng, H., 2019. Early-Holocene monsoon instability and climatic optimum recorded by Chinese stalagmites. The Holocene 29, 1059-1067.

Yuan, D., Cheng, H., Edwards, R.L., Dykoski, C.A., Kelly, M.J., Zhang, M., Qing, J., Lin, Y., Wang, Y., Wu, J., Dorale, J.A., An, Z., Cai, Y., 2004. Timing, Duration, and Transitions of the Last Interglacial Asian Monsoon. Science 304, 575-578.

Zhang, D., 2003. Climatic Differences in China during the Holocene Indicated by the Various Climatic Proxy Data from Different Parts of China. Journal of Glaciology and Geocryology, 25(1): 11-18.

Zhang, N., Yang, Y., Cheng, H., Zhao, J., Yang, X., Liang, S., Nie, X., Zhang, Y., Edwards, R.L., 2018. Timing and duration of the East Asian summer monsoon maximum during the Holocene based on stalagmite data from North China. The Holocene 28, 1631-1641.

Zhang, P., Cheng, H., Edwards, R.L., Chen, F., Wang, Y., Yang, X., Liu, J., Tan, M., Wang, X., Liu, J., An, C., Dai, Z., Zhou, J., Zhang, D., Jia, J., Jin, L., Johnson, K.R., 2008. A Test of Climate, Sun, and Culture Relationships from an 1810-Year Chinese Cave Record. Science 322, 940-942.

Zhao, J., Cheng, H., Yang, Y., Tan, L., Spötl, C., Ning, Y., Zhang, H., Cheng, X., Sun, Z., Li, X., Li, H., Liu, W., Edwards, R.L., 2019. Reconstructing the western boundary variability of the Western Pacific Subtropical High over the past 200 years via Chinese cave oxygen isotope records. Climate Dynamics 52, 3741-3757.

Zhou, X., Sun, L., Zhan, T., Huang, W., Zhou, X., Hao, Q., Wang, Y., He, X., Zhao, C., Zhang, J., 2016. Time-transgressive onset of the Holocene Optimum in the East Asian monsoon region. Earth and Planetary Science Letters 456, 39-46.

Figure 1.

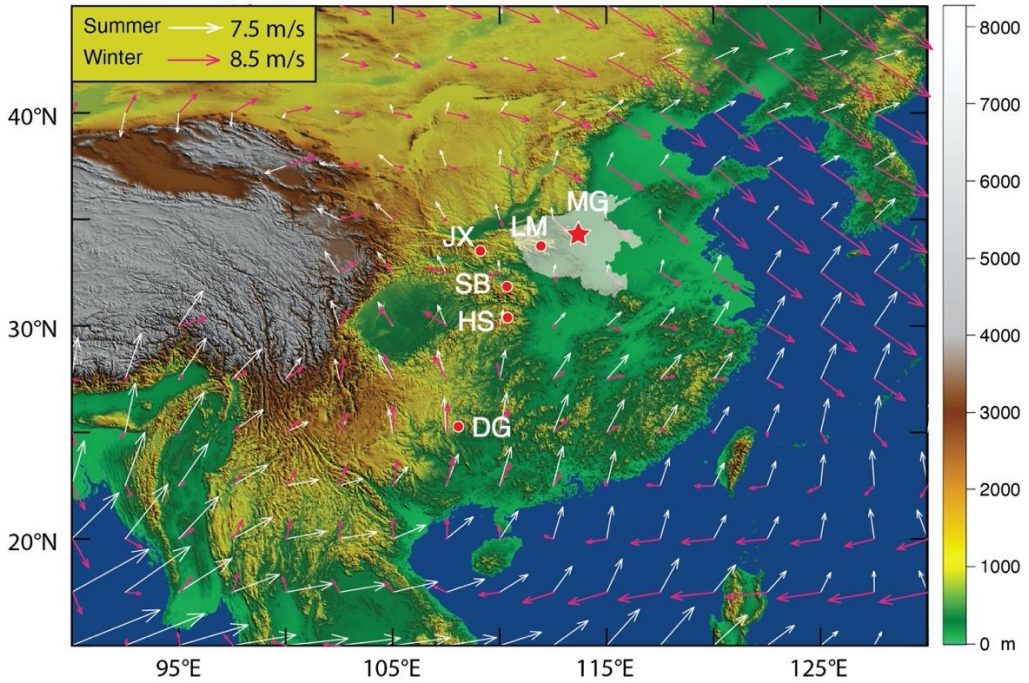

Figure 1: Overview map with the location of the studied cave and relevant records. The topographic map is based on GTOPO 30 data (U.S. Geological Survey's EROS (Earth Resources Observation and Science; http://eros.usgs.gov/#/Find_Data/Products_and_Data _Available/gtopo30_info) Data Center). White and purple arrows indicate mean summer and winter wind fields at 850 hPa from 1981 to 2010 (NCEP Reanalysis Derived data provided by NOAA/OAR/ESRL PSD, Boulder, Colorado, USA, http://www.esrl.noaa.gov/psd/, Kistler et al., 2001). The location of Magou Cave (MG) is denoted by the red star (113°23'E, 34°19'N, ~422 m a.s.l.), all other records are denoted by red circles: LM: Laomu Cave/Dongshiya Cave, 111°31'E, 33°48'N, ~840 m a.s.l.; JX: Jiuxian Cave, 109°6'E, 33°34'N, ~1495 m a.s.l.; SB: Sanbao Cave, 110°26'E, 31°40'N, ~1900 m a.s.l.; HS: Heshang Cave, 110°25'E, 30°27'N, ~294 m a.s.l.; DG: Dongge Cave, 108°5'E, 25°17'N, ~680 m a.s.l. The white shaded area indicates the Henan Province, largely representing the Central Plain of China.

Figure 2.

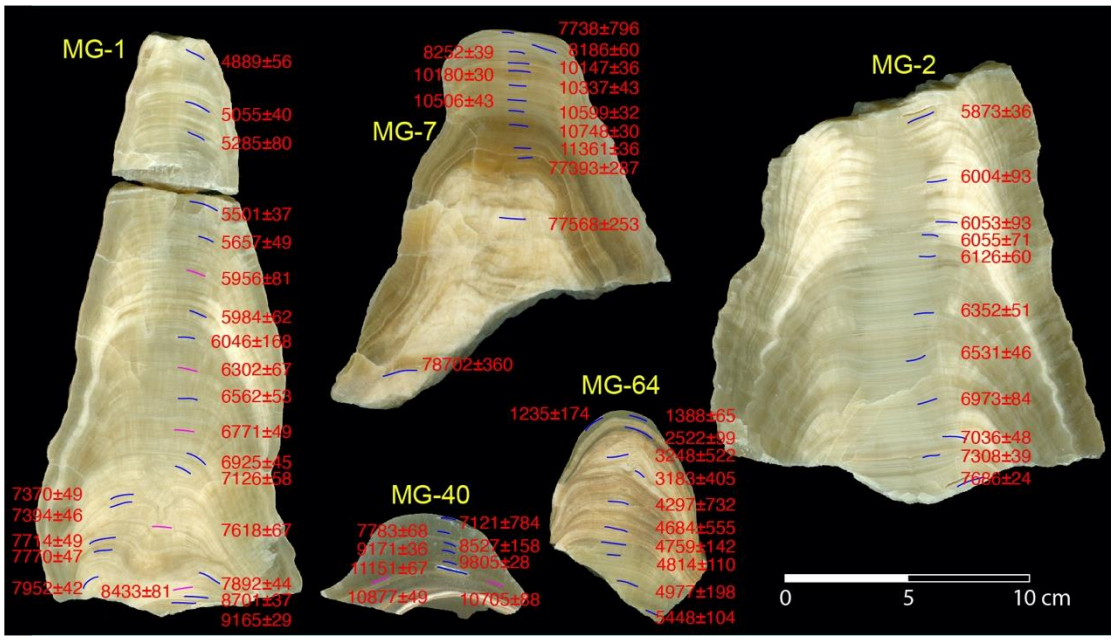

Figure 2: Overview with scanned cross-sections of stalagmites MG-1, MG-2, MG-7, MG-40 and MG-64. ^{230}Th dates are indicated in red next to the drilled slits. Drill spots shown in light purple indicate newly taken dating samples added in MG-1 and MG-40 in this study.

952 Figure 3.
953

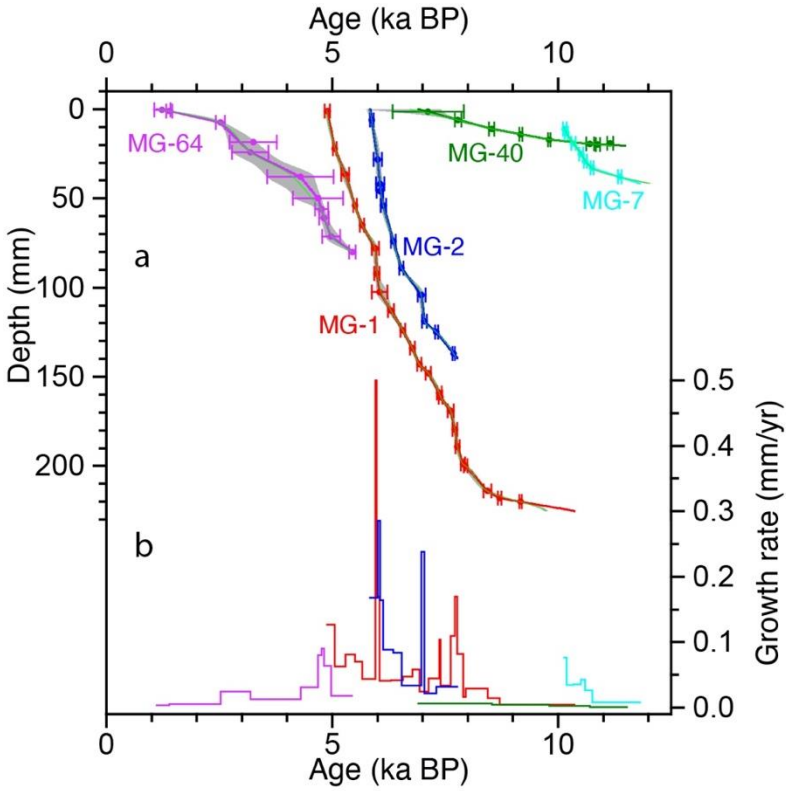

954
955
956 **Figure 3:** Age-depth models (a) and grow rate time series (b) for stalagmites MG-1,
957 MG-2, MG-7, MG-40 and MG-64. All ages of the stalagmites are reported as
958 thousand years before present (1950 AD), ka BP. The indicated age errors are 2σ
959 error. Both the linear interpolation and COPRA pchip models are used to calculate the
960 chronologies of all these stalagmites. The chronological differences between both
961 approaches are negligible because of the high density of dates and relatively small
962 dating errors (most errors are <1%). Different colors denote individual stalagmites.
963

964 Figure 4.
965

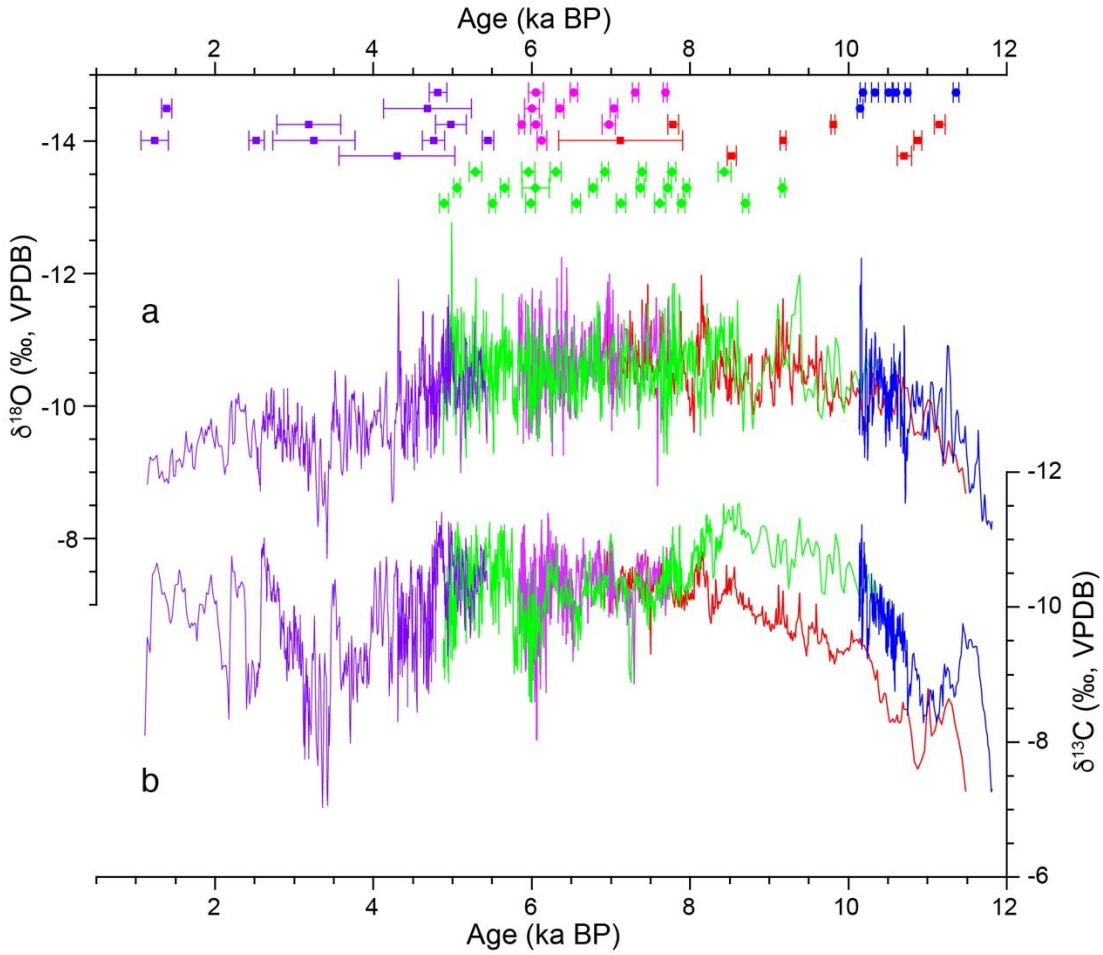

966
967
968 **Figure 4:** The individual time series of speleothem $\delta^{18}O$ (a) and $\delta^{13}C$ (b) obtained
969 from Magou Cave. The ^{230}Th dates are shown with 2σ error. The different stalagmites
970 are color-coded, MG-1 is shown in green; MG-2 in pink; MG-7 in blue; MG-40 in
971 red; and MG-64 in purple.
972

973 Figure 5.

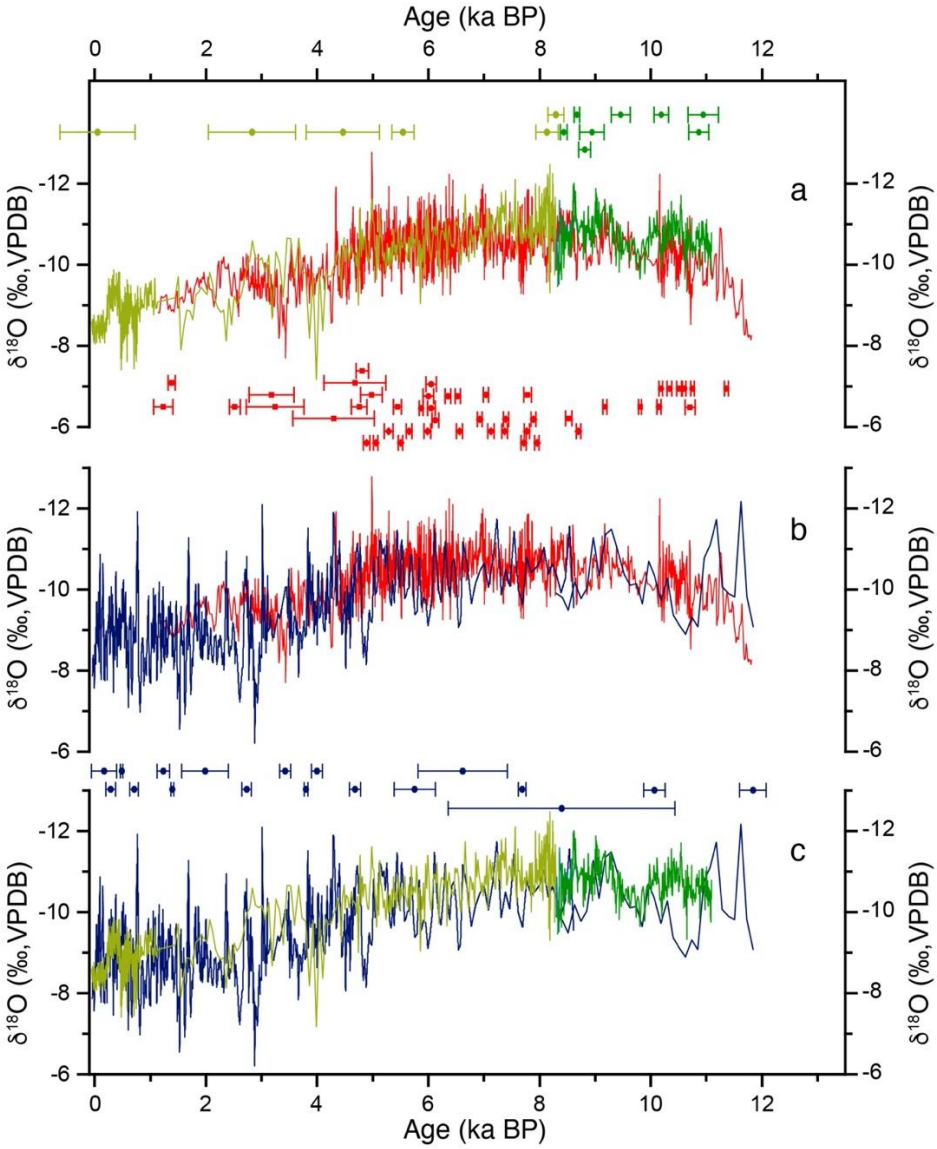

974
975

976 **Figure 5:** Comparisons of the MG composite $\delta^{18}O$ record and other speleothem $\delta^{18}O$ time
977 series from central China. a) the MG composite $\delta^{18}O$ record (red, this study) and the $\delta^{18}O$
978 record of the Laomudong/Dongshiya Caves (green for Dongshiya Cave and yellow green for
979 Laomudong Cave, Zhang et al., 2018); b) the MG composite $\delta^{18}O$ record (red, this study) and
980 the $\delta^{18}O$ record from Jiuxian Cave (blue, Cai et al., 2010); c) the $\delta^{18}O$ records from Jiuxian
981 Cave (blue, Cai et al., 2010) and the Laomudong/Dongshiya Caves (green for Dongshiya
982 Cave and yellow green for Laomudong Cave, Zhang et al., 2018). ^{230}Th dates with 2 σ errors
983 of each record from different caves are also shown and color-coded by using the same color
984 as the $\delta^{18}O$ record.

985 Figure 6.
986

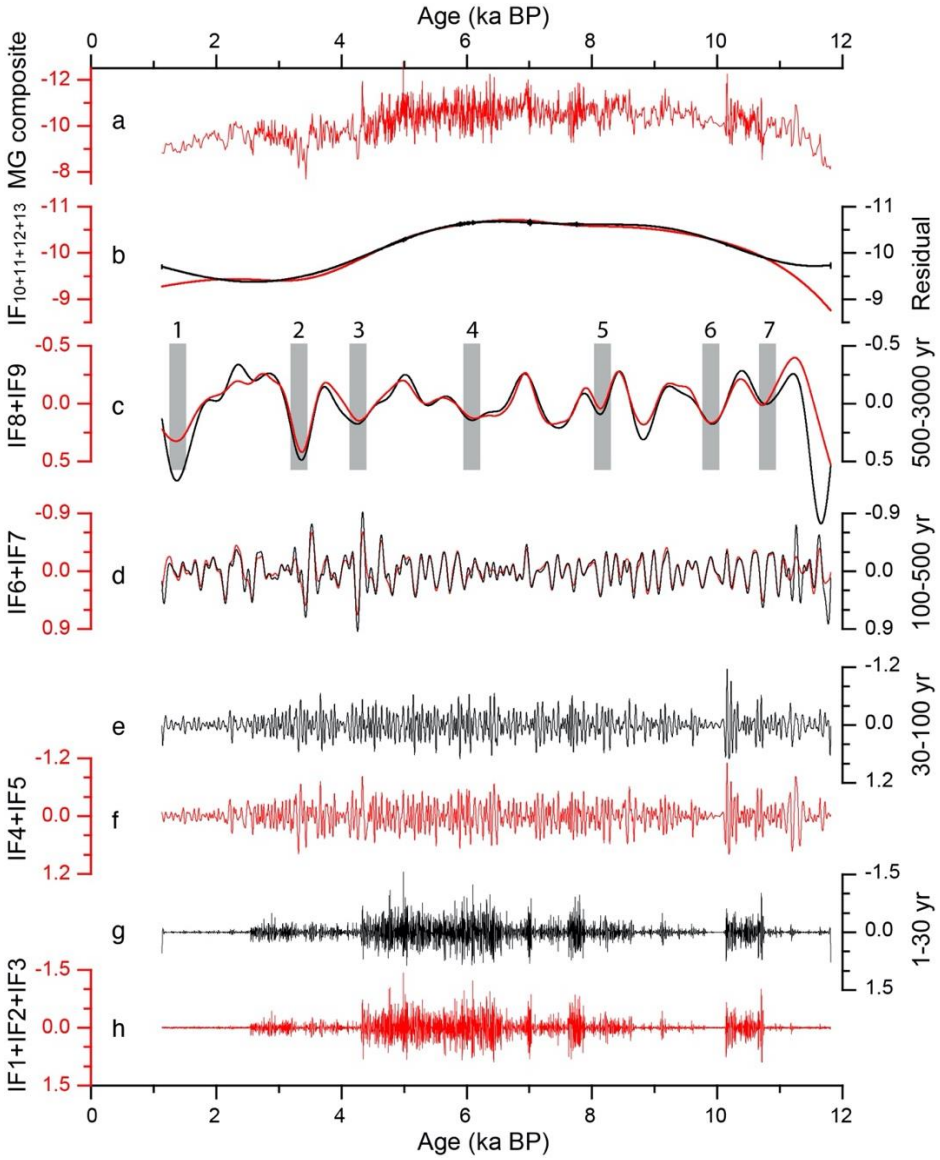

987
988
989 **Figure 6:** The MG composite time series (a) from ~11.7-1.1 ka BP and derived EEMD
990 components (red) and wavelet band-pass components (black) (b-h). For the EEMD
991 decomposition, noise of 0.2 standard deviations of the data is added for the ensemble
992 calculation, with an ensemble number is 500. Five EEMD components (i.e. sum of
993 components 1-3, sum of components 4-5, sum of components 6-7, sum of components 8-9,
994 and sum of components 10-13) are presented. The wavelet band-pass components indicate the
995 variation of speleothem $\delta^{18}O$ on different timescales and correspond well with the EEMD
996 components.

997 Figure 7.

998

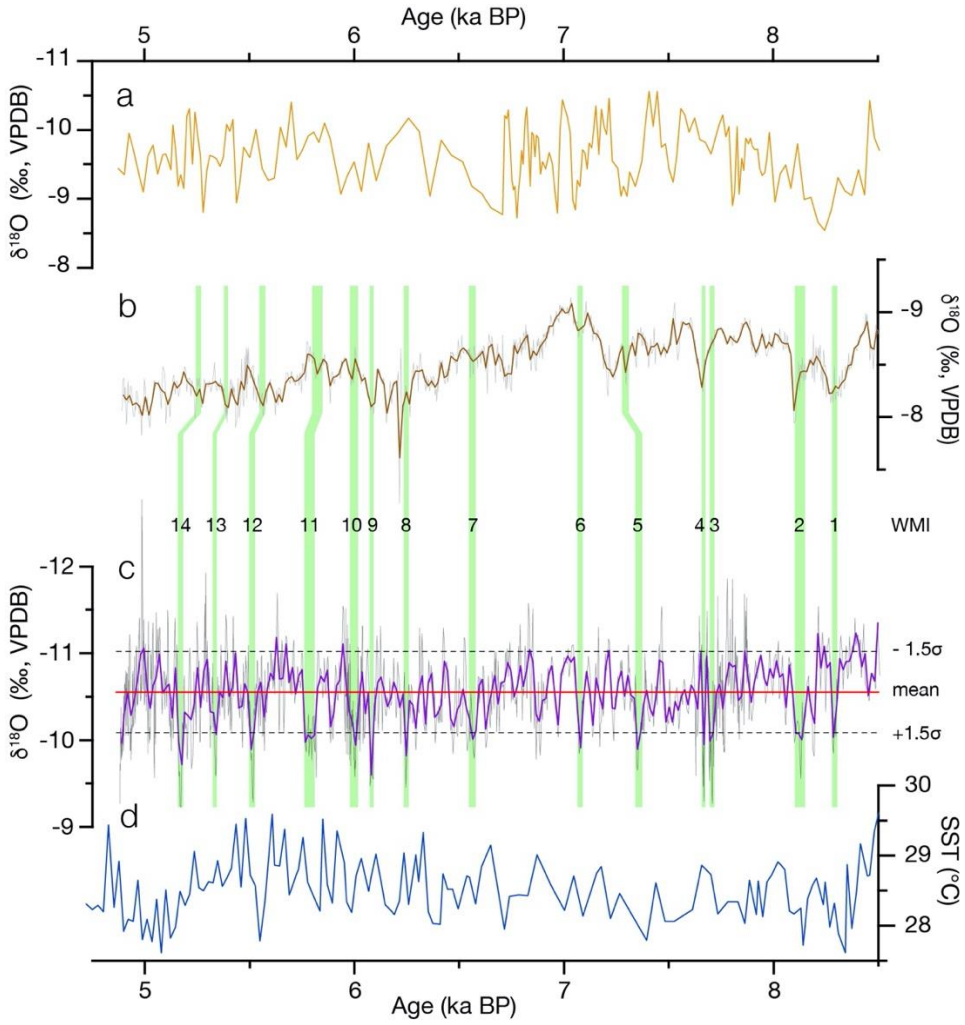

999

1000 **Figure 7:** Comparison of speleothem $\delta^{18}O$ records and west Pacific warm pool sea surface

1001 temperature (SST) during the Holocene megathermal (8.5 to 4.8 ka BP). a) the speleothem

1002 $\delta^{18}O$ record from Heshang Cave; b) the speleothem $\delta^{18}O$ record from Dongge Cave. The

1003 brown line represents the 15-year weighted-average time series. c) the speleothem $\delta^{18}O$

1004 record from Magou Cave. The purple line represents the 15-year weighted-average time

1005 series, in which we identify 14 weak summer monsoon intervals (numbered green shades)

1006 using a threshold of ±1.5 standard deviations from the mean $\delta^{18}O$. d) the SST time series

1007 obtained from drill core MD-98-2178 (Fan et al., 2018).

1008 Figure 8.

1009

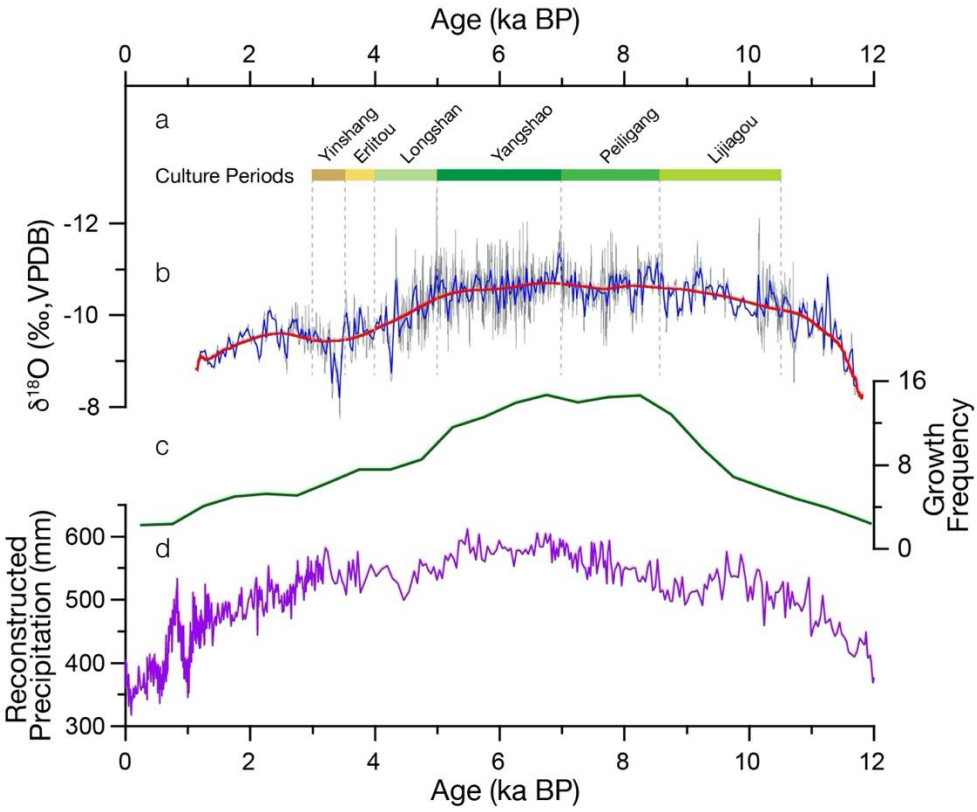

1010

1011

1012 **Figure 8:** The MG composite time series of stalagmite $\delta^{18}O$ (b, this study), the growth

1013 frequency record of Longfeng Cave (c, Wei et al., 2020), the reconstructed precipitation using

1014 the fossil pollen assemblages from Gonghai Lake (d, Chen et al., 2015) and ancient cultural

1015 periods as observed in Henan Province, central China (a, Li et al., 2015a). The grey, blue and

1016 red lines denote the original, 30-years adjacent-averaged and 2000-year weighted-average

1017 curves of MG composite record, respectively. The color bars indicate different archeological

1018 culture periods.